JCB Journal of Cell Biology

REPORT

SIK3 suppresses neuronal hyperexcitability by regulating the glial capacity to buffer K^+ and water

Hailun Li[1], Alexandra Russo[1], and Aaron DiAntonio[1,2]

Glial regulation of extracellular potassium (K^+) helps to maintain appropriate levels of neuronal excitability. While channels and transporters mediating K^+ and water transport are known, little is understood about upstream regulatory mechanisms controlling the glial capacity to buffer K^+ and osmotically obliged water. Here we identify salt-inducible kinase 3 (SIK3) as the central node in a signal transduction pathway controlling glial K^+ and water homeostasis in *Drosophila*. Loss of SIK3 leads to dramatic extracellular fluid accumulation in nerves, neuronal hyperexcitability, and seizures. SIK3-dependent phenotypes are exacerbated by K^+ stress. SIK3 promotes the cytosolic localization of HDAC4, thereby relieving inhibition of Mef2-dependent transcription of K^+ and water transport molecules. This transcriptional program controls the glial capacity to regulate K^+ and water homeostasis and modulate neuronal excitability. We identify HDAC4 as a candidate therapeutic target in this pathway, whose inhibition can enhance the K^+ buffering capacity of glia, which may be useful in diseases of dysregulated K^+ homeostasis and hyperexcitability.

Introduction

Neuronal excitability is tightly coupled to complex ion dynamics in the nervous system. As ions move, so too must osmotically obliged water molecules move. Following bursts of action potentials, ionic gradients are restored via active transport. Defects in water and ion homeostasis disrupt neuronal firing and can result in edema (Rusan et al., 2014; Byun and Delpire, 2007). Potassium (K^+) homeostasis is particularly important for maintaining the physiological function of neurons (Kofuji and Newman, 2004). Repolarization of the axonal membrane during action potentials transfers K^+ ions into the extracellular space. With synchronous activity, the bulk extracellular [K^+] rises, and this K^+ must be rapidly buffered via glial and/or neurons lest axons depolarize, disrupting neuronal firing.

Glial cells are essential for potassium and water homeostasis (Bellot-Saez et al., 2017; Kofuji and Newman, 2004). Glia remove K^+ ions from the extracellular space and redistribute them to areas with lower [K^+] to maintain ionic gradients. Glia also express aquaporin water channels to functionally couple K^+ clearance and water transport, thereby relieving osmotic stress. A number of K^+ and water transport molecules mediate glial regulation of extracellular [K^+], including K^+ channels, Na^+-K^+-Cl^- cotransporter 1, Na^+-K^+-ATPase, and aquaporin 4 (Larsen et al., 2014; Strohschein et al., 2011; Weiss et al., 2019). Defects in glial transporters can result in build-up of ions in the extracellular space between axons and glia, leading to extracellular fluid accumulation. Indeed, mouse and *Drosophila melanogaster* mutants with defective K^+ transport exhibit dramatic and strikingly similar edema phenotypes in their peripheral nerves (Byun and Delpire, 2007; Leiserson et al., 2000). These swellings correlate with seizure sensitivity and offer an elegant readout for identifying molecules that are required to maintain ionic and water homeostasis and a healthy level of neuronal excitability.

While much is known about the key transporters and channels that mediate the flux of water and ions (Djukic et al., 2007; Jayakumar et al., 2011; Larsen et al., 2014; Leiserson et al., 2011, 2000; MacVicar et al., 2002; Papadopoulos et al., 2004; Rusan et al., 2014; Stenesen et al., 2019; Wu et al., 2014), the mechanisms by which glial cells regulate expression of the relevant transporters are not well understood. Delineating such regulatory mechanisms could identify approaches to leverage glial K^+ and water buffering as a therapeutic strategy for neuroprotection against K^+ stress-related damage. We conducted a glial-specific screen in *Drosophila* and identified a signal transduction pathway required for glial regulation of water and ion homeostasis. This screen uncovered a central role for salt-inducible kinase 3 (SIK3), a highly conserved AMP-activated protein kinase (AMPK)–family kinase that links signal sensing

[1]Department of Developmental Biology, Washington University in St. Louis School of Medicine, St. Louis, MO; [2]Needleman Center for Neurometabolism and Axonal Therapeutics, Washington University in St. Louis School of Medicine, St. Louis, MO.

Correspondence to Aaron DiAntonio: diantonio@wustl.edu.

to changes in cellular response (Choi et al., 2015; Sasagawa et al., 2012; Uebi et al., 2012; Wang et al., 2011). Loss of SIK3 in glia results in nerve edema, neuronal hyperexcitability, and increased seizure susceptibility, all phenotypes that are commonly associated with human genetic disorders disrupting glial water and ion homeostasis (Min and van der Knaap, 2018). This swelling phenotype is critically and selectively sensitive to K^+ stress. Moreover, we demonstrate that SIK3 functions via regulation of a downstream HDAC4/Mef2 transcriptional program that controls expression of relevant ion and water transporters. HDAC4 is a critical negative regulator in the pathway, and pharmacological inhibition of HDAC4 potently suppresses the edema, hyperexcitability, and seizure phenotypes of *SIK3* mutants. Hence, this study identifies a druggable pathway controlling the glial capacity to buffer K^+ and water and a candidate therapeutic approach to achieve the long-standing goal of targeting glia for the control of hyperexcitability (Devinsky et al., 2013; Heuser et al., 2014).

Results and discussion

SIK3 in glia restricts extracellular fluid accumulation in the *Drosophila* peripheral nervous system

Glia remove K^+ from the extracellular space to maintain ionic and water homeostasis in the nervous system. Disrupting K^+ buffering leads to nerve edema, neuronal hyperexcitability, and increased seizure susceptibility. In *Drosophila*, loss of glial K^+ transport function results in characteristic focal peripheral nerve swellings due to accumulation of extracellular fluid (Leiserson et al., 2000; Rusan et al., 2014). To identify signaling pathways required for glial regulation of K^+ and water homeostasis, we performed an in vivo glial-specific screen in *Drosophila*. We employed the pan-glial driver Repo-GAL4 to express a library of ∼500 RNAi lines targeting signaling molecules (Table S1), and screened for genes that are required to prevent swelling of larval peripheral nerves. From the screen we found a single hit: glial knockdown of the gene for SIK3 results in pronounced nerve swellings.

Peripheral nerves from wild-type larvae have a uniform diameter, with an average width (W) of 6.2 ± 1.1 µm, and never show swellings. Peripheral nerves from larvae in which SIK3 is knocked down in glia have 24 ± 1.3 focal nerve swellings per larva with an average width of 30 ± 2.1 µm and length (L) of 67 ± 5.2 µm (n = 10; Fig. 1 A). Glial knockdown of SIK3 using a second, nonoverlapping RNAi transgene gives the same phenotype (Fig. S1 B). Null alleles of *SIK3* are lethal; however, there is a strong hypomorphic *SIK3* allele ($SIK3^{\Delta 48}$) that survives to the third instar larval stage (Wang et al., 2011). $SIK3^{\Delta 48}$ larvae exhibit a similar but more pronounced nerve swelling phenotype, with larger (W: 68 ± 3.2 µm, L: 140 ± 9.5 µm) and more frequent swellings (44 ± 3.4 per larva, n = 12). Our findings from the RNAi screen point to an essential function of SIK3 in glia. To test whether the more dramatic phenotype in the bona fide mutant reflects a glial function for SIK3, we tested rescue with a SIK3 transgene expressed from either a glial (Repo-Gal4) or neuronal (Elav-Gal4) promoter. Nerve swellings in *SIK3* mutants are fully rescued by glial-specific expression of SIK3, while neuronal expression of SIK3 has no effects on the swelling phenotype (Fig. 1 B). Moreover, knockdown of SIK3 selectively in neurons does not induce nerve swellings (Fig. S1 C). Hence, SIK3 is required in glia but not neurons to suppress nerve swellings.

Drosophila peripheral nerves include three types of glia—wrapping glia directly ensheathe the axons, while subperipeurial and perineurial glia participate in formation of the blood–brain barrier (Stork et al., 2008). To determine which glial subtype requires SIK3, we employed subtype-specific GAL4 drivers for both rescue and knockdown of SIK3. Wrapping glia-specific expression of SIK3 with Nrv2-Gal4 robustly rescues the mutant phenotype, abolishing almost all nerve swellings (Fig. 1 C). In contrast, expressing SIK3 with Gli-Gal4 in the subperineurial glia partially suppresses the swelling phenotype, and SIK3 expression with 46F-Gal4 in the perineurial glia does not suppress. In complementary experiments, we used the same set of GAL4 drivers to knock down SIK3 in each glial layer. SIK3 knockdown in wrapping glia induces the characteristic nerve swelling phenotype, while knockdown of SIK3 in the other two subtypes does not alter peripheral nerve morphology (Fig. S1, D–F). These results demonstrate that SIK3 may have a modest role in subperineural glia, but primarily functions in wrapping glia to suppress nerve swellings. Since wrapping glia directly ensheathe axons, this finding suggests that SIK3 may regulate ion and water homeostasis in the extracellular space between axonal and glial membranes.

To test the hypothesis that SIK3 regulates extracellular fluid accumulation between glia and axon, we performed EM analysis on peripheral nerves from wild-type and *SIK3* mutant larvae ($SIK3^{\Delta 48}$). In wild-type nerves, glia tightly ensheathe axons (Fig. 1 D). In contrast, large electron transparent regions (*) are present in *SIK3* mutants in the extracellular space between glia and axons (Fig. 1, E–G; and Fig. S1, K and L). Some swellings are huge, nearly filling the entire swollen nerve (Fig. 1 F, note difference in scale). Similar results are seen when knocking down SIK3 in glia labeled with cytoplasmic RFP—thin optical sections reveal large unstained swellings surrounded by glia as expected for extracellular accumulation of fluid (Fig. S1, I and J). Axons persist within these massive swellings and appear to be morphologically normal (Fig. 1 G, arrow). As a second test of axonal integrity, we expressed a membrane-targeted GFP in a small subset of neurons with or without glial knockdown of SIK3. Axons appear defasciculated yet intact within the swellings of *SIK3* mutant nerves (Fig. S1, G and H). These phenotypes resemble but are much more dramatic than those of *fray* mutants, where extracellular nerve edema is caused by loss of a kinase that regulates a glial K^+ transporter (Leiserson and Keshishian, 2011). We find that null mutants of *fray* exhibit 17 ± 1.4 nerve swellings per larva (W: 20 ± 1.6 µm, L: 60 ± 4.7 µm, n = 12), which is consistent with prior findings. Nerve swellings are much larger and more frequent in the absence of SIK3 than Fray, so SIK3 may play a more central role in the regulation of ion and water homeostasis.

Glial SIK3 modulates neuronal excitability via K^+ regulation

K^+ flux across neurons and glia is a major determinant of fluid accumulation in the extracellular space, and the nerve edema

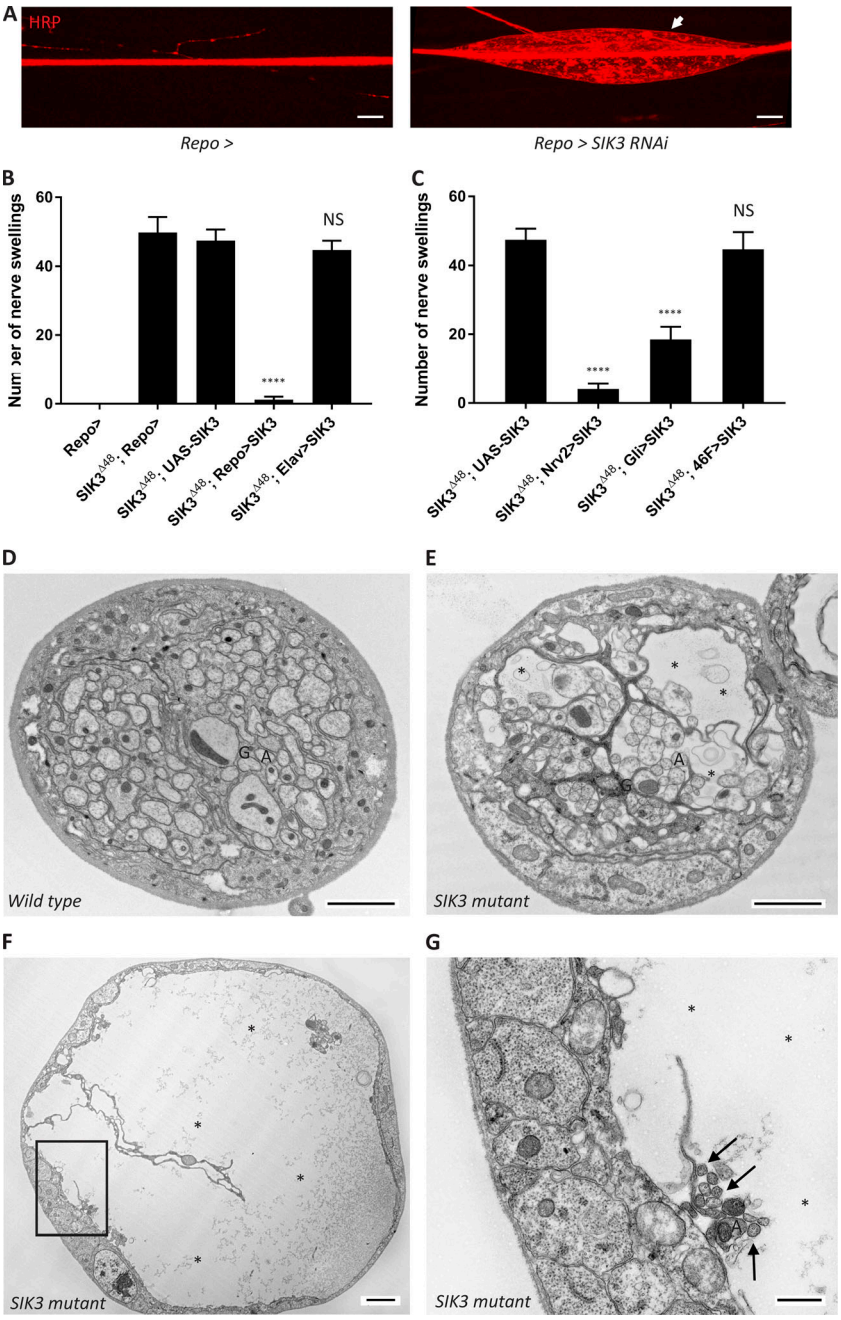

Figure 1. **Glial SIK3 prevents extracellular nerve edema. (A)** Representative images of peripheral nerves in third instar larvae stained for the nerve membrane marker HRP. The pan-glial driver Repo-GAL4 was used to express a UAS-GFP transgene (control; abbreviated as *Repo>*) or SIK3 RNAi (*Repo>SIK3 RNAi; UAS-SIK3 RNAi no. 1* was used unless otherwise noted). Loss of SIK3 from glia induces localized nerve swellings (arrow). Scale bars, 20 µm. **(B)** Quantification of nerve swellings in control, $SIK3^{\Delta 48}$ mutants, and mutants with SIK3 expression in glia or neurons. Control larvae (*Repo>*) do not display swellings. $SIK3^{\Delta 48}$ mutants ($SIK3^{\Delta 48}$*;Repo>*, $SIK3^{\Delta 48}$*;UAS-SIK3*) exhibit swellings that resemble A; swellings are rescued by expression of UAS-SIK3 in glia (*Repo>SIK3*), but not in neurons (*Elav>SIK3*). $n \geq 30$. One-way ANOVA with Tukey's multiple comparisons; ****, $P < 0.0001$; NS, $P > 0.05$. Data are mean ± SEM. **(C)** Quantification of nerve swellings in $SIK3^{\Delta 48}$ mutant with UAS-SIK3 either in the absence of a GAL4 driver ($SIK3^{\Delta 48}$*;UAS-SIK3*) or expression in wrapping glia (*Nrv2>SIK3*), subperineurial glia (*Gli>SIK3*) or perineurial glia (*46F>SIK3*). Nerve swellings in $SIK3^{\Delta 48}$ larvae are suppressed when SIK3 is expressed in wrapping glia or subperineurial glia. $n \geq 20$. One-way ANOVA with Tukey's multiple comparisons; ****, $P < 0.0001$; NS, $P > 0.05$. **(D–G)** Representative EM sections through peripheral nerves. The axons (examples labeled "A") are tightly ensheathed by surrounding glia (examples labeled "G") in wild type (D), but axons and glia are separated by large extracellular swellings (asterisks) in $SIK3^{\Delta 48}$ larvae (E–G). Details of boxed region in F are shown in G. Axons are denoted by arrows. Scale bars, 2 µm for D–F, 500 nm for G.

present in *SIK3* mutants resembles that of mutants with altered K^+ transport (Byun and Delpire, 2007; Leiserson and Keshishian, 2011). To test the hypothesis that glial SIK3 is required for proper K^+ homeostasis, we provided a K^+ stress by raising third instar larvae on a diet supplemented with either 200 mM KCl or NaCl and examined peripheral nerve morphology. Nerves of wild-type larvae raised on a high K^+ diet appear uniform with an average width comparable to those raised on control diet (Fig. S2 A). In contrast, a high K^+ diet dramatically exacerbates the nerve defects observed in larvae with glial-specific SIK3 knockdown, enhancing both the number and the size of the swellings (Fig. 2, A–C). Moreover, this phenotype is also enhanced when these larvae are raised on a diet containing two other K^+ salts (200 mM KCH_3CO_2 or KH_3PO_4; Fig. S2, B–D). In contrast, a high Na^+ diet had no impact on the number or size of swellings (Fig. 2, B and C). Hence, SIK3 is required for an effective glial response to a K^+ stress.

K^+ dynamics play a critical role in modulating neuronal activity, and dysfunctional glial K^+ regulation promotes neuronal hyperexcitability in seizure patients and in mouse and fly models of seizure (Bedner et al., 2015; Weiss et al., 2019). Here we tested whether glial SIK3 has a non-cell autonomous impact on axonal excitability at the larval neuromuscular junction (NMJ). In this system, the peripheral nerve is severed so no action potentials propagate from the motor neuron cell bodies and so no evoked synaptic potentials are recorded from the muscle without exogenous nerve stimulation. We detect miniature excitatory junctional potentials (mEJPs) in muscles of

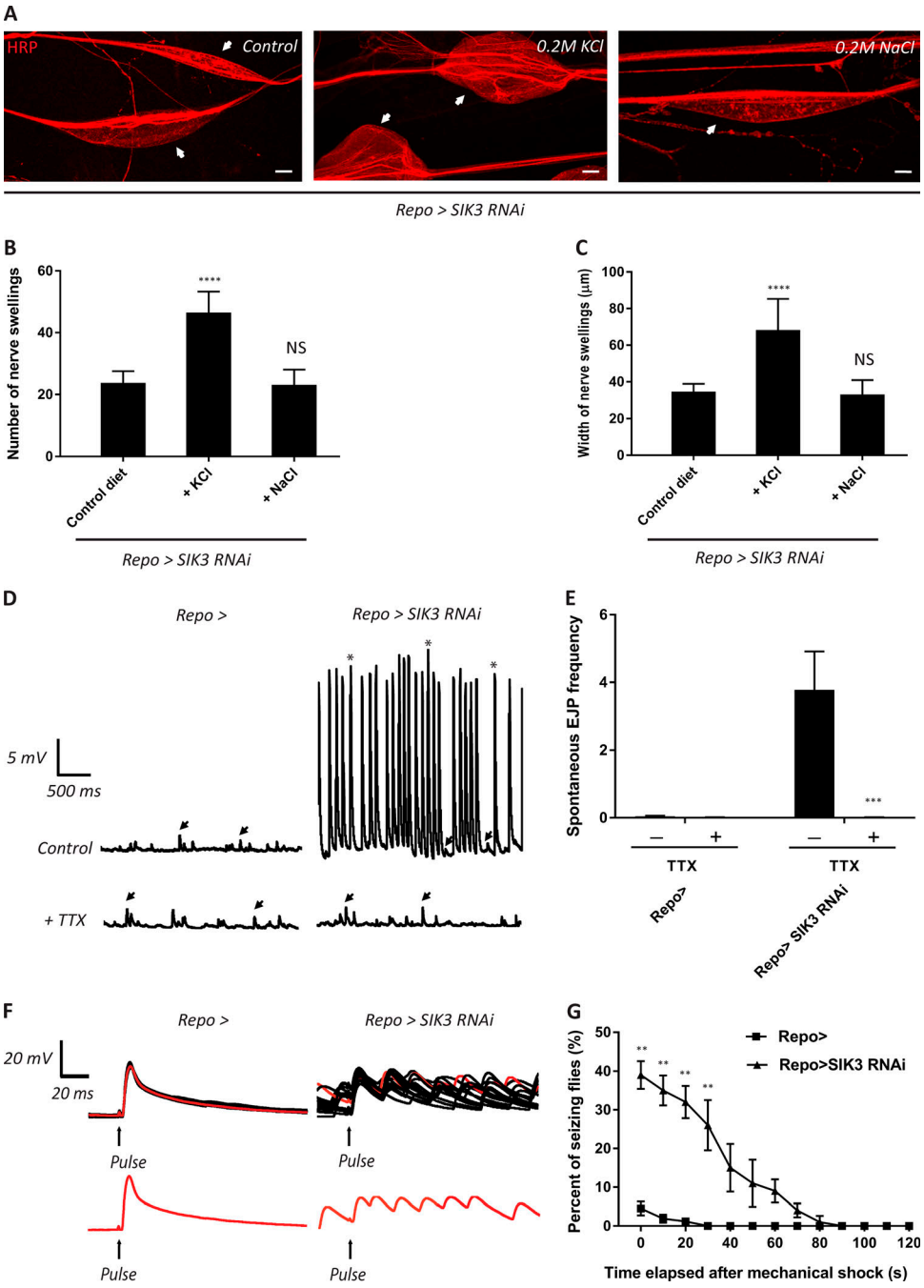

Figure 2. **Glial SIK3 protects from K⁺ stress and suppresses neuronal hyperexcitability and seizure sensitivity. (A)** Representative images of nerves with pan-glial knockdown of SIK3 in larvae fed a high-salt diet. Swellings are denoted by arrows. Scale bars, 20 µm. **(B and C)** Quantifications of nerve swellings in SIK3 RNAi-expressing larvae raised on control, KCl- (200 mM) or NaCl-rich (200 mM) diet. KCl- but not NaCl-rich diet significantly increases the number (B) and the width (C) of nerve swellings. $n \geq 20$. One-way ANOVA with Tukey's multiple comparisons; ****, $P < 0.0001$; NS, $P > 0.05$. **(D)** Representative physiological traces recorded from larval NMJs. Control larvae (*Repo>*) only have mEJPs (arrowheads), whereas larvae expressing SIK3 RNAi in glia exhibit both mEJPS and spontaneous EJPs (asterisks) that are sensitive to TTX. **(E)** Quantification of frequency of spontaneous EJPs for genotypes in D. Over 50 consecutive events were analyzed over a passive recording window (up to 75 consecutive events or 120 s, whichever occurred first), and events with amplitudes ≥4 mV were considered spontaneous EJPs. Before TTX: $n = 9$; after TTX: $n = 4$. Two-way ANOVA with Tukey's multiple comparisons; ***, $P < 0.001$. **(F)** Representative EJP traces recorded from larval NMJs. Top: Overlaid traces of evoked response triggered by 75 consecutive pulses (arrow) in a given cell; the number of EJPs ranges from 7 to 129 per cell. Bottom: Evoked response caused by a single pulse. $n = 7$ for *Repo>*; $n = 10$ for *Repo>SIK3 RNAi*. **(G)** Time course of vortex-induced seizure behaviors in control and SIK3 RNAi-expressing flies. $n \geq 10$ groups of 10 flies per genotype for each time point. Two-tailed Student's *t* test; **, $P < 0.01$. Data are mean ± SEM.

wild-type larvae, due to the spontaneous release of single synaptic vesicles, but no evoked events (Fig. 2, D and E). When recording from larvae in which SIK3 is knocked down in glia, we detect both mEJPs as well as much larger events that appear to be evoked junctional potentials (EJPs). To test whether these large synaptic events are indeed evoked and action potential dependent, we treated with tetradotoxin (TTX), a Na^+ channel blocker that inhibits the firing of action potentials. TTX completely suppresses the large synaptic events present with glial SIK3 knockdown, leaving only mEJPs (Fig. 2, D and E). Hence, loss of SIK3 in glia allows motor axons to fire spontaneous action potentials, a hallmark of neuronal hyperexcitability.

Having demonstrated that glial SIK3 suppresses spontaneous action potential firing in motor axons, we next assessed the response of these axons to exogenous stimulation. Following nerve stimulation, wild-type motor axons fire a single action potential that triggers an EJP. Each stimulus triggers a single EJP (seen in 7 of 7 cells; Fig. 2 F). In contrast, upon glial SIK3 knockdown, a single stimulus still triggers an EJP, but can also trigger supernumerary EJPs (ranging from 7 to 129 events per cell, seen in 7 of 10 cells). While the number of EJPs is abnormal, the average amplitude of each EJP does not differ from wild type, suggesting that evoked synaptic release properties remain largely unchanged (Fig. S3, A and B). These phenotypes of spontaneous firing in the absence of stimulation and supernumerary responses to single stimuli are characteristic of hyperexcitable K^+ channel mutants such as *eag shaker* (Ganetzky and Wu, 1983). We conclude glial SIK3 suppresses axonal excitability.

Genetic mutations that cause neuronal hyperexcitability can induce seizures in both humans and *Drosophila* (Noebels et al., 2012; Parker et al., 2011). Here we tested whether glial-specific knockdown of SIK3 increases seizure susceptibility as assessed by bang sensitivity, a test of response to mechanical stimulation (Kuebler et al., 2001; Pavlidis and Tanouye, 1995). Following a 20-s mechanical shock to adult flies, we recorded the incidence of seizing behaviors including shuddering, leg shaking, contorted posturing, and spinning flight. This stimulus does not elicit seizure behavior in the vast majority of control flies, and in those few flies that do show seizure behavior, it lasts only seconds. In contrast, with glial SIK3 knockdown, ∼40% of flies show seizure behavior, and this behavior can persist for more than a minute (Fig. 2 G). Hence, glial SIK3 suppresses seizure susceptibility. Taken together, we find that glial SIK3 is required to maintain proper K^+ and water homeostasis in the nerve, axonal excitability, and seizure resistance. Due to this central and previously unappreciated role for glial SIK3, we next sought to define its downstream effectors in glia.

SIK3 regulates HDAC4 nucleo-cytoplasmic localization in glia to promote K^+ and water homeostasis

SIK3 is a highly conserved AMPK-related kinase that often regulates downstream transcriptional programs. In *Drosophila*, SIK3 can influence gene expression by phosphorylating and thereby regulating the nucleo-cytoplasmic localization of HDAC4, whose unphosphorylated form transits to the nucleus, where it can bind and inhibit transcription factors (Fujii et al., 2017; Wang et al., 2011). To test whether this is the mechanism of action of SIK3 in glia, we first tested whether the kinase activity of SIK3 is required for its function. While expression of wild-type SIK3 in glia fully rescues the nerve swelling phenotype of $SIK3^{\Delta 48}$ larvae, expression of a kinase-dead SIK3 (SIK3.K70M) fails to rescue nerve swellings (Fig. 3 A). Hence, glial SIK3 acts through its canonical function as a kinase. We hypothesize that HDAC4 is a key SIK3 substrate and that phosphorylation negatively regulates HDAC4 function. If so, then HDAC4 would be required for the *SIK3* mutant phenotype, and excess HDAC4 would phenocopy the *SIK3* mutant phenotype. Consistent with this model, glial-specific knockdown of HDAC4 does not influence gross nerve morphology in otherwise wild-type larvae, but fully rescues the nerve swelling phenotype of $SIK3^{\Delta 48}$ larvae (Fig. 3 A). Moreover, HDAC4 overexpression in glia recapitulates the nerve swelling phenotype observed in *SIK3* mutants (Fig. 3 B; compare to Fig. 2 B control diet). If HDAC4 acts downstream of SIK3, then these HDAC4-dependent swellings should be influenced by SIK3 activity. Indeed, HDAC4 overexpression-induced swellings are exacerbated by glial knockdown of SIK3, and are completely suppressed by SIK3 overexpression (Fig. 3 B). Finally, larvae that overexpress a phosphorylation-defective form of HDAC4 (HDAC4.3A) have significantly more swelling defects than those overexpressing wild-type HDAC4, and a similar number to those in which wild-type HDAC4 is overexpressed but SIK3 is knocked down (Fig. 3 B). Taken together, we conclude that SIK3 suppresses HDAC4 activity in glia to promote K^+ and water homeostasis.

To explore the cell biological mechanism by which SIK3 regulates HDAC4 function, we tested the model that active SIK3 sequesters HDAC4 in the cytoplasm. We coexpressed a nuclear-localized GFP to label nuclei with a FLAG-tagged HDAC4 in glia to assess HDAC4 localization, and then measured HDAC4 intensity in both the nucleus and cytoplasm and calculated a nuclear:cytoplasmic HDAC4 ratio (Fig. 3, C and D). To test if SIK3 regulates HDAC4 localization, we knocked down or overexpressed SIK3 in glia expressing FLAG-HDAC4. Knockdown of SIK3 greatly enhances HDAC4 localization to glial nuclei, while SIK3 overexpression promotes exclusion of HDAC4 from the nucleus. SIK3 loss-of-function (LOF) and gain-of-function result in an approximately fivefold increase and decrease in the nuclear:cytoplasmic HDAC4 ratio, respectively (Fig. 3, C and D). Moreover, this SIK3 regulation of HDAC4 localization correlates closely with SIK3-dependent modulation of HDAC4-induced nerve swellings. Loss of SIK3 promotes nuclear localization of HDAC4 and enhances nerve swellings, while overexpression of SIK3 inhibits nuclear localization of HDAC4 and suppresses nerve swellings (Fig. 3, B–D). We conclude that SIK3 promotes glial K^+ and water homeostasis by regulating HDAC4 nucleo-cytoplasmic localization, and that nerve swellings and HDAC4 localization are two complementary readouts of SIK3 activity.

SIK3 regulates Mef2-dependent glial expression of ion and water transporters

Having demonstrated that SIK3 sequesters HDAC4 in the glial cytoplasm, we investigated the mechanism by which nuclear HDAC4 disrupts K^+ and water homeostasis. HDAC4 regulates a

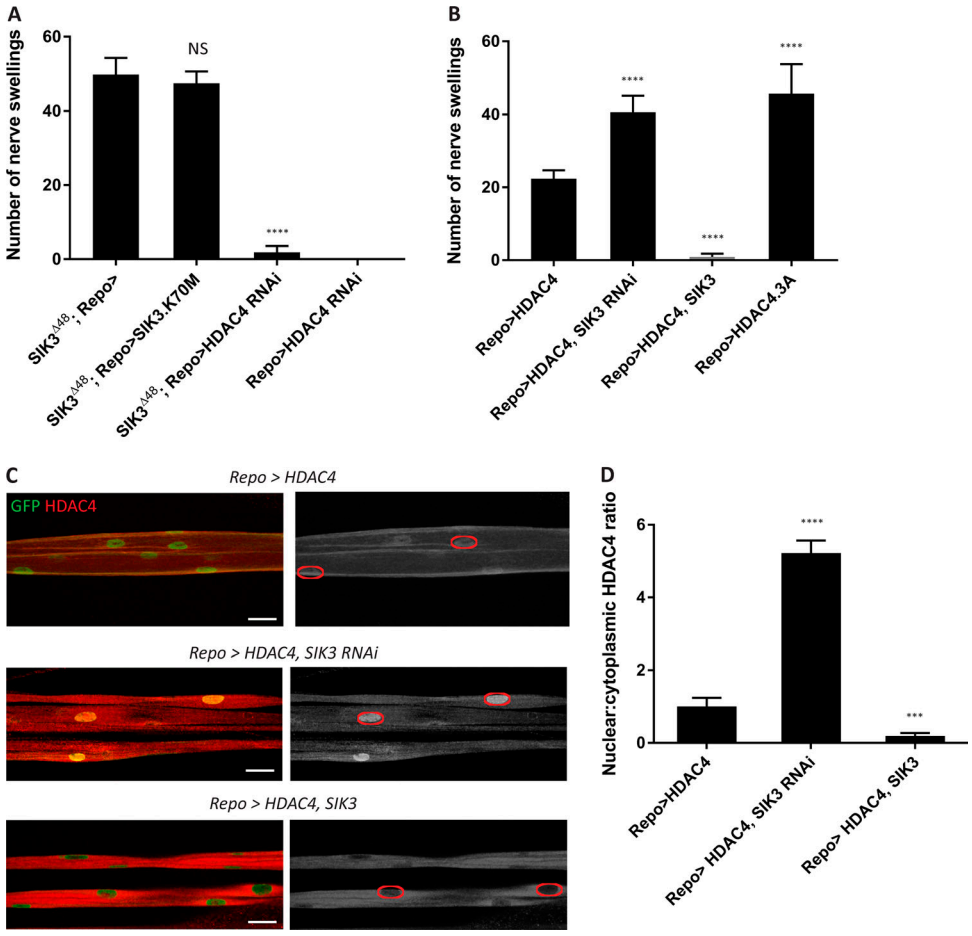

Figure 3. **Glial SIK3 regulates the nuclear shuttling of HDAC4 to suppress nerve swellings. (A)** Quantification of nerve swellings in *SIK3*$^{\Delta 48}$ mutant with glial expression of UAS-GFP as control (*Repo>*), catalytically inactive SIK3 (*Repo>SIK3.K70M*) or HDAC4 RNAi (*Repo>HDAC4 RNAi*). $n \geq 20$. One-way ANOVA with Tukey's multiple comparisons; ****, $P < 0.0001$; NS, $P > 0.05$. **(B)** Quantification of nerve swellings in larvae with HDAC4 overexpression (*Repo>HDAC4*), HDAC4 overexpression, and SIK3 knockdown (*Repo>HDAC4,SIK3 RNAi*), HDAC4 and SIK3 overexpression (*Repo>HDAC4,SIK3*), or expression of nuclear-localizing HDAC4 (*Repo>HDAC4.3A*). $n \geq 20$. One-way ANOVA with Tukey's multiple comparisons; ****, $P < 0.0001$. **(C)** Representative images of nerves demonstrating the effects of SIK3 depletion and overexpression on HDAC4 localization in glia. Left: Glial nuclei (green) and HDAC4 (red). Right: Grayscale images show HDAC4 staining; glial nuclei are outlined. Scale bars, 15 µm. **(D)** Quantification of nuclear:cytoplasmic ratio of HDAC4 for genotypes in C. $n \geq 20$ larvae per genotype. Data are presented as fold changes relative to *Repo>HDAC4*. One-way ANOVA with Tukey's multiple comparisons; ***, $P < 0.001$; ****, $P < 0.0001$. Data are mean ± SEM.

number of transcription factors, including forkhead box protein O, cAMP response element-binding protein, Sima, and Mef2 in *Drosophila* (Schwartz et al., 2016; Wang et al., 2014). To identify the relevant target, we overexpressed or knocked down each candidate above in glia with Repo-GAL4 and assessed peripheral nerve morphology. From this mini-screen, only RNAi-mediated knockdown of Mef2 recapitulates the nerve swelling phenotype of SIK3 knockdown, suggesting that Mef2 is required for K^+ and water homeostasis in glia and is inhibited by nuclear HDAC4 (Fig. 4 A). Consistent with this model, HDAC4 represses Mef2-dependent transcriptional activity in other tissues in both *Drosophila* and mice (Fitzsimons et al., 2013; Sando et al., 2012). If Mef2 functions downstream of SIK3-HDAC4, then its overexpression in glia should suppress the *SIK3* mutant phenotype. Indeed, overexpression of Mef2 in wrapping glia, the glial subtype that requires SIK3, suppresses the swelling defects in *SIK3* mutants (Fig. 4 B). Moreover, knockdown of HDAC4 in wrapping glia also suppresses the *SIK3* nerve swelling phenotype (Fig. 4 B). Together, these complementary LOF and gain-of-function studies with Mef2 and HDAC4 strongly support the model that SIK3 sequesters HDAC4 in the cytoplasm of wrapping glia to enable Mef2 to promote proper K^+ and water homeostasis. Interestingly, HDAC hyperactivity and Mef2 deficiency have been associated with seizure in mice and human, respectively (Phiel et al., 2001; Paciorkowski et al., 2013). Having demonstrated a role for Mef2 in the SIK3 signaling pathway, we next investigated Mef2 transcriptional targets that may directly mediate the regulation of K^+ and water.

Mef2 regulates the transcription of over 300 genes in *Drosophila* (Sivachenko et al., 2013; Sandmann et al., 2006), and we hypothesized that some of these Mef2 targets promote glial K^+ and water homeostasis. To identify candidates, we selected genes that are regulated by Mef2 and have known roles in K^+ and/or water transport. We identified two such candidates, *fray*

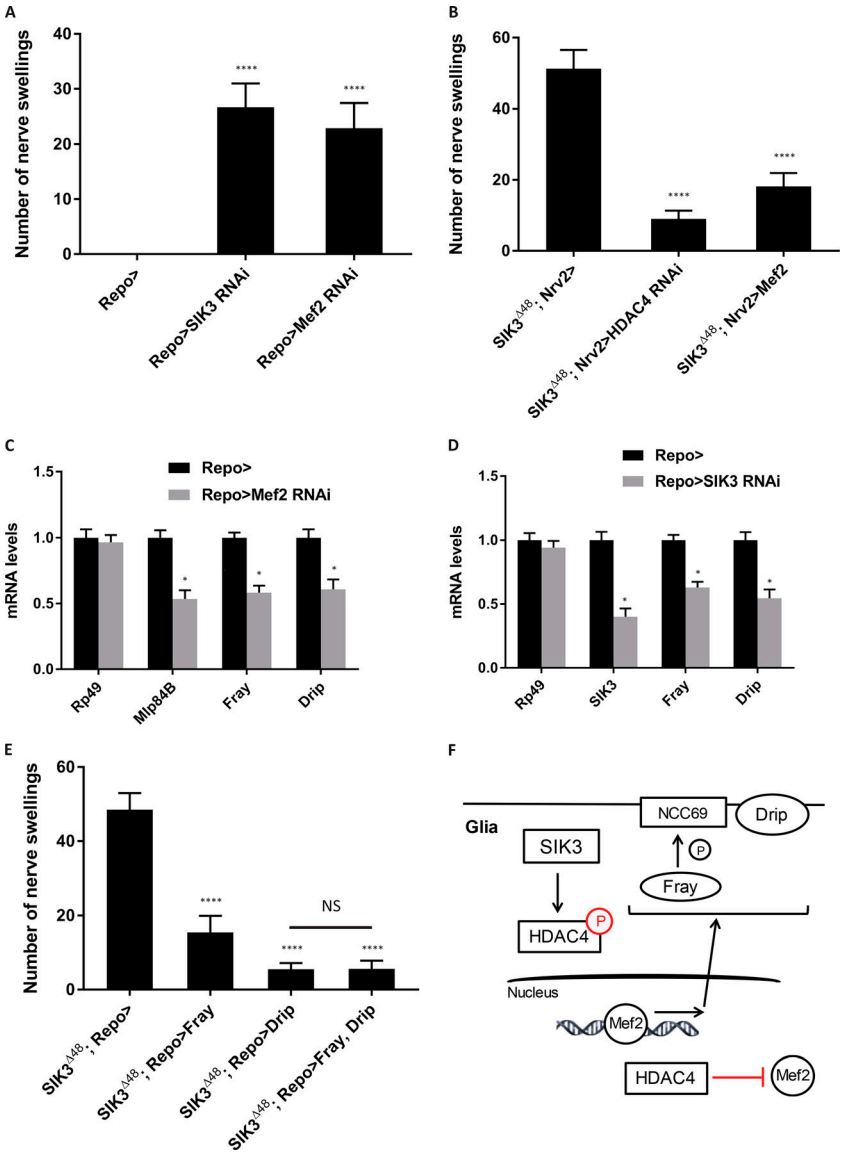

Figure 4. **Mef2 functions downstream of SIK3 to control expression of ion and water transporters in glia. (A)** Quantification of nerve swellings in larvae with glial expression of UAS-GFP as control (*Repo>*), SIK3 RNAi or Mef2 RNAi. $n \geq 30$. One-way ANOVA with Tukey's multiple comparisons; ****, $P < 0.0001$. **(B)** Quantification of nerve swellings in $SIK3^{\Delta 48}$ mutant with wrapping glia-specific expression of UAS-GFP (*Nrv2>*), HDAC4 RNAi (*Nrv2>HDAC4 RNAi*) or wild-type Mef2 (*Nrv2>Mef2*). $n = 15$. One-way ANOVA with Tukey's multiple comparisons; ****, $P < 0.0001$. **(C)** Quantitative PCR analysis of mRNA levels of a reference gene (*rp49*), Mef2 protein-coding gene (*mlp84B*), *fray* and *drip* in ventral nerve cords (VNCs) of control larvae (*Repo>*) and those with Mef2-depleted glia. $n = 3$ independent experiments. Data are normalized to *rp49* and presented as fold changes relative to the control. Two-tailed Student's *t* test; *, $P < 0.05$. **(D)** Quantitative PCR analysis of mRNA levels of *rp49*, *sik3*, *fray*, and *drip* in VNCs of control larvae and those with SIK3-depleted glia. $n = 3$ independent experiments. Two-tailed Student's *t* test; *, $P < 0.05$. **(E)** Quantification of nerve swellings in $SIK3^{\Delta 48}$ mutant with pan-glial expression of UAS-GFP (*Repo>*), UAS-Fray, UAS-Drip, or coexpression of UAS-Fray and UAS-Drip. $n = 10$. One-way ANOVA with Tukey's multiple comparisons; ****, $P < 0.0001$. **(F)** Schematic model of SIK3-mediated regulation of ion and water homeostasis: SIK3 functions through a HDAC4-Mef2 signaling axis to regulate the transcription of *fray* and *drip*, which regulate the glial capacity to buffer K^+ and water. Phosphorylation is indicated by "P." All data are mean ± SEM.

and *drip*. *Fray* encodes a kinase that activates the Na^+-K^+-Cl^- cotransporter NCC69 in fly glia, and mutations in either *fray* or *ncc69* cause nerve swellings that resemble *SIK3* mutants (Leiserson et al., 2000; Rusan et al., 2014). *Drip* is the fly orthologue of aquaporin 4, which in mammals is predominantly expressed in astrocytes and may play a key role in epileptogenesis (Lee et al., 2012). To test whether *fray* and *drip* are downstream of SIK3-HDAC4-Mef2 signaling pathway in glia, we used quantitative PCR to confirm that mRNA levels of *fray*, *drip*, and *mlp84B*, a well-characterized Mef2 transcriptional target (Stronach et al., 1999), are significantly reduced in larvae with glial knockdown of Mef2 (Fig. 4 C). The mRNA levels of a reference gene, *rp49*, were comparable between the two genotypes. We next tested whether *fray* and *drip* mRNA levels are down when SIK3 is knocked down exclusively in glia. Because PNS glia are not easily accessible for mRNA analysis, we used ventral nerve cords isolated from larvae with glial-specific knockdown of SIK3. We confirmed SIK3 knockdown, and demonstrated that mRNA levels of *fray* and *drip* are significantly decreased compared with wild-type larvae (Fig. 4 D). There is an ∼40% loss of both genes, but knockdown of SIK3 only occurred in glia, while mRNA was prepared from both neurons and glia, so the actual degree of knockdown in glia is likely an underestimate. We conclude that the SIK3-HDAC4-Mef2 signaling pathway regulates glial expression of *fray* and *drip*, which likely contribute to the glial capacity to transport K^+ and water.

To test directly if *fray* and *drip* are functionally relevant targets of the SIK3 pathway, we conducted glial-specific rescue experiments in the *SIK3* mutant background. Loss of SIK3 in glia decreases expression of *fray* and *drip*, so if they function downstream of SIK3, then expressing *fray* or *drip* in glia should suppress the mutant phenotype. We used upstream activating sequence (UAS) fray and drip transgenes under the control of Repo-Gal4 to limit expression to glia and to bypass the Mef2 requirement for expression of the endogenous genes. In support of our hypothesis, glial expression of *fray* in the $SIK3^{\Delta 48}$ mutant leads to a 68% decrease in the swelling defects (Fig. 4 E). Glial overexpression of *drip* suppresses the $SIK3^{\Delta 48}$ mutant phenotype

even more strongly, decreasing the number of swellings by ~88%. Co-expression of *fray* and *drip* in the *SIK3*$^{\Delta 48}$ mutant suppresses no better than expression of *drip* alone, suggesting that Drip may act downstream of Fray to control water transport and fluid accumulation (Fig. 4 E). These findings suggest a unified model for the role of the SIK3 pathway in glial K^+ and water homeostasis. Active SIK3 phosphorylates HDAC4 to sequester it in the cytoplasm, promoting a Mef2-dependent gene expression program required for proper K^+ and water homeostasis in glia. Two central components of this program are (1) Fray, the activating kinase of a Na^+-K^+-Cl^- cotransporter that facilitates glial uptake of K^+, and (2) Drip, a water channel that helps alleviate the osmotic stress caused by K^+ flux (Fig. 4 F).

Pharmacological inhibition of HDAC4 reverts SIK3-induced hyperexcitability

Having defined this SIK3-HDAC4-Mef2 pathway, we next tested whether this program can be modulated pharmacologically to enhance the glial capacity to maintain K^+ and water homeostasis. HDAC4 is the central negative regulator in this pathway, and is effectively inhibited by the class I/II histone deacetylase inhibitor trichostatin A (TSA) in *Drosophila* fat body (Wang et al., 2011). We tested whether chemical inhibition of HDACs including HDAC4 with TSA can suppress the SIK3 LOF phenotypes in glia. Wild-type and *SIK3*$^{\Delta 48}$ larvae were raised on food supplemented with 10 µM TSA. While no changes were observed in wild-type larvae, TSA blocks the development of nerve swellings in *SIK3*$^{\Delta 48}$ mutants (Fig. 5 A). This suppression is as effective as glial-specific knockdown of HDAC4 (compare to Fig. 3 A). Next, we tested the efficacy of TSA for suppression of neuronal hyperexcitability induced by glial knockdown of SIK3. We raised wild-type larvae on food with or without 10 µM TSA, and found no difference in evoked synaptic transmission (Fig. S3, C and D), demonstrating that TSA does not alter the ability to trigger an action potential or evoke synaptic release. We then raised control larvae and larvae with glial knockdown of SIK3 on food with or without TSA supplementation. TSA supplementation suppressed the hyperexcitability induced by glial SIK3 knockdown, blocking both spontaneous firing of motor axons (Fig. 5, B and C) and supernumerary events following a single stimulus (Fig. 5 D). Hence, pharmacological inhibition of HDAC suppresses hyperexcitability, likely via restoration of glial K^+ and water homeostasis. Finally, we investigated if TSA could suppress the increased seizure susceptibility induced by SIK3 knockdown in glia. Much of the adult nervous system forms during pupal development, when the animal does not eat and so cannot be fed TSA. Hence, we asked if treatment with TSA only in adulthood could suppress seizures. Larvae with glial knockdown of SIK3 were raised on a control diet and, as adults, were moved onto either control or TSA-containing food for 2 d before being tested for seizure behaviors. TSA treatment decreased the proportion of flies exhibiting seizure behaviors by ~50% (Fig. 5 E). Hence, pharmacological inhibition of HDACs exclusively in adulthood suppresses SIK3 LOF-induced seizures. Interestingly, HDAC inhibition is a therapeutic strategy to prevent the onset and persistence of seizure (Reddy et al., 2018). Valproic acid is a pan-HDAC inhibitor that has been widely used to treat epilepsies (Phiel et al., 2001). Although several pathways have been proposed to underlie its antiepileptic function, its mechanism of action is not fully understood. Our data suggest that the efficacy of HDAC inhibitors may involve activation of glial mechanisms that boost K^+ and water homeostasis and suppress neuronal excitability.

Materials and methods

Drosophila stocks and genetics

Flies were cultured using standard techniques, and all crosses were maintained at 25°C in 60% relative humidity. The following stocks were used in this study: *SIK3*$^{\Delta 48}$ (strong hypomorphic allele of *SIK3*), UAS-SIK3, UAS-SIK3.K70M (catalytically inactive SIK3), UAS-HDAC4, UAS-HDAC4.3A (nuclear localizing HDAC4), gifts from B. Wang, University of California, San Francisco, CA (Wang et al., 2011); UAS-Mef2 (Blanchard et al., 2010; a gift from J. Blau, New York University, NY); UAS-Fray (Leiserson et al., 2011; a gift from H. Keshishian, Yale University, CT); UAS-Drip-Venus (Cabrero et al., 2014; a gift from J. Dow, University of Glasgow, UK); Gli-GAL4 (Auld et al., 1995) and 46F-GAL4 (Xie and Auld, 2011), gifts from V. Auld, The University of British Columbia, Canada; and ppk-CD4-GFP (Han et al., 2011; a gift from Y.N. Jan, University of California, San Francisco, CA). Flies obtained from the Bloomington *Drosophila* Stock Center include Repo-GAL4 (Sepp et al., 2001), Elav-GAL4 (Yao and White, 1994), Nrv2-GAL4 (Sun et al., 1999), UAS-nls:GFP (RRID:BDSC_4775), UAS-SIK3 RNAi no. 2 (RRID:BDSC_57302), UAS-HDAC4 RNAi (RRID:BDSC_28549, BDSC_34774), UAS-Mef2 RNAi (RRID:BDSC_28699, BDSC_38247), UAS-Fray RNAi (RRID:BDSC_55878), and UAS-LexA RNAi (RRID:BDSC_67945). UAS-SIK3 RNAi no. 1 (KK 106268) was obtained from the Vienna *Drosophila* Resource Center. Both UAS-SIK3 RNAi lines target all isoforms of SIK3. In all GAL4 experiments, control animals were generated by crossing virgins of the respective driver to UAS-GFP or UAS-LexA RNAi males.

Immunocytochemistry

Third instar larvae were dissected in 4°C PBS and fixed either in Bouin's fixative for 10 min at room temperature or in 4% paraformaldehyde for 20 min at 4°C. Upon fixation, larval preps were washed three times for 10 min with PBS + 0.1% Triton X-100 (PBST) and blocked in PBST with 5% goat serum for 30 min. To assess peripheral nerve morphology, larvae were incubated in Cy3-conjugated goat α-HRP antibody (Jackson ImmunoResearch; 123–165-021; RRID:AB_2338959) at 1:1,000 dilution for 60 min at room temperature. To assess HDAC4 localization and glial/axonal morphology, larvae were incubated overnight at 4°C in primary antibodies, including mouse α-FLAG antibody (Sigma-Aldrich; F3165; RRID:AB_259529) at 1:1,000 dilution and rabbit α-RFP (Clontech; 632496; RRID: AB_10013483) at 1:500 dilution. On the next day, larvae were washed with PBST and incubated for 90 min at room temperature in the following secondary antibodies: Cy3 goat α-mouse (1:1,000; Jackson ImmunoResearch; 115–165-146; RRID: AB_2338680), Cy3 goat α-rabbit (1:1,000; Invitrogen; A-10520; AB_2534029), and Alexa Fluor 488–conjugated goat α-rabbit (1:1,000; Invitrogen; A-

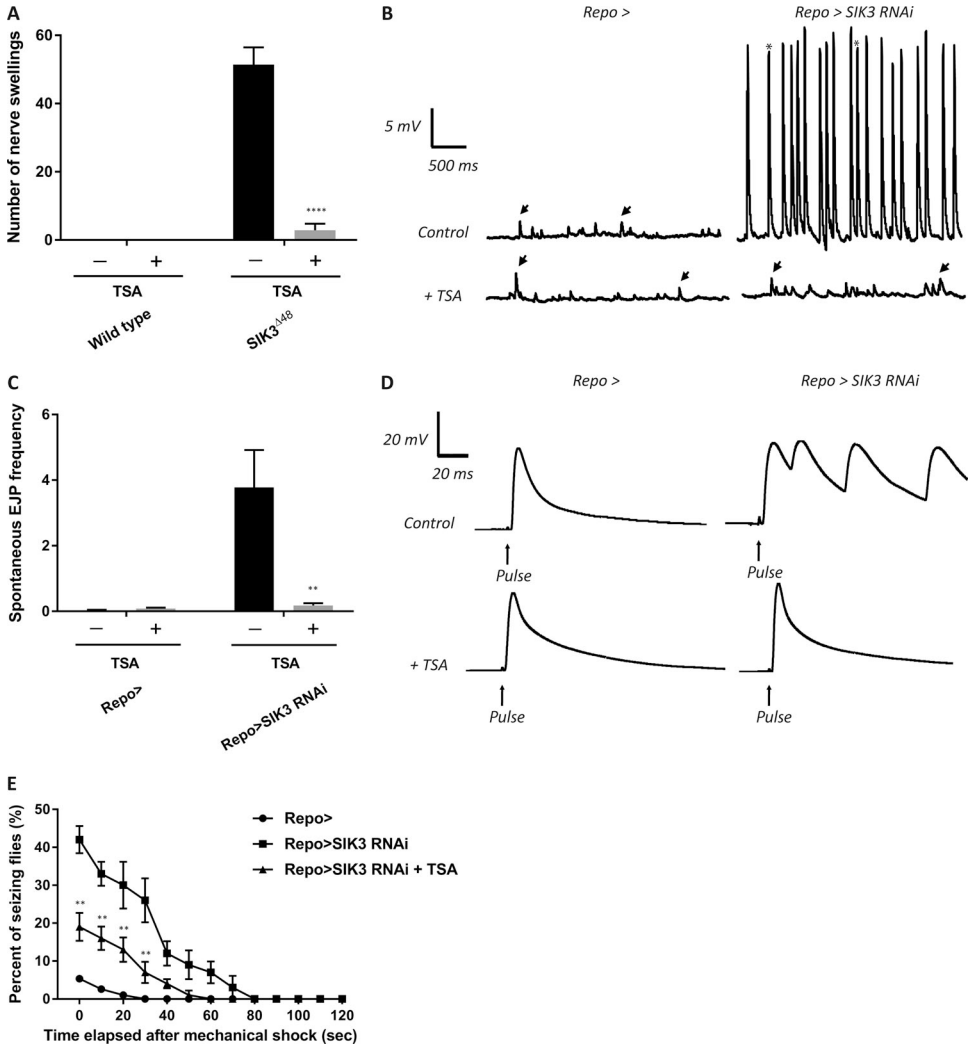

Figure 5. **Pharmacological inhibition of HDAC4 suppresses neuronal hyperexcitability and seizure susceptibility of *SIK3* mutants. (A)** Quantification of nerve swellings in wild-type and $SIK3^{\Delta 48}$ mutant larvae raised on control or TSA-containing (10 µM) diet. TSA, a pan-HDAC inhibitor, completely rescues the nerve defects in *SIK3* mutants. $n = 20$. Two-way ANOVA with Tukey's multiple comparisons; ****, $P < 0.0001$. **(B)** Representative physiological traces recorded from larval NMJs. Spontaneous EJPs (asterisks) caused by loss of SIK3 from glia are suppressed in larvae fed TSA-containing diet. These events do not occur in control larvae (*Repo>*) that display only mEJPs (arrowheads). **(C)** Quantification of frequency of spontaneous EJPs for genotypes in B. Events with amplitudes ≥4 mV were considered spontaneous EJPs, and the spontaneous EJP frequencies were averaged per genotype per condition. Control diet: $n = 9$ for *Repo>*, $n = 9$ for *Repo>SIK3 RNAi*; TSA-rich diet: $n = 9$ for *Repo>*, $n = 8$ for *Repo>SIK3 RNAi*. Two-way ANOVA with Tukey's multiple comparisons; **, $P < 0.01$. **(D)** Representative EJP traces recorded from larval NMJs. TSA suppresses the supernumerary evoked events in SIK3 RNAi-expressing larvae following a stimulus without impacting the evoked response of controls. Control diet: $n = 8$ for *Repo>*, $n = 10$ for *Repo>SIK3 RNAi*; TSA-rich diet: $n = 8$ for *Repo>*, $n = 8$ for *Repo>SIK3 RNAi*. **(E)** Time course of vortex-induced seizure behaviors in control and SIK3 RNAi-expressing flies fed control or TSA-containing diet as adults. $n \geq 5$ groups of 10 flies per genotype for each time point. Two-tailed Student's *t* test; **, $P < 0.01$. Data are mean ± SEM.

11034; RRID: AB_2576217). Following incubation with secondary antibodies, larval preps were washed with PBST and equilibrated in 70% glycerol in PBS overnight at 4°C. Larvae were mounted and imaged in Vectashield (Vector Laboratories) the next day.

Imaging and analysis

Peripheral nerve morphology

Larvae stained for α-HRP were examined and imaged using 20×/0.60 NA and 40×/1.15 NA oil immersion objectives on a Leica TCS SPE confocal microscope equipped with the Leica DFC7000 T camera and the LAS X software. For a given experiment, images for all genotypes and conditions were acquired at room temperature at one sitting using identical laser power, gain, and offset settings with the same step size. Unless otherwise noted, images shown are maximal Z-projections of confocal stacks. Thin consecutive optical sections were used to highlight extracellular swellings in peripheral nerves. Acquired images were minimally processed using Photoshop CC (2.2; Adobe) and Illustrator (15.0.0; Adobe) to prepare for final figures. To quantify nerve swellings, nerves between segments A2 to A8 were traced from the ventral nerve cord to their branch points in the periphery. Regions with a maximum nerve width larger than 15 µm were scored and counted as swellings. The

total number of nerve swellings was measured for each larva and averaged per each genotype per condition.

HDAC4 localization

Larvae that express FLAG-tagged HDAC4 in glia were stained for HDAC4 and GFP-labeled glial nuclei. Peripheral nerves were imaged using the 40×/1.15 NA oil immersion objective on the confocal microscope at room temperature. For each experiment, images were taken using identical settings and shown as maximal Z-projections of confocal stacks. Acquired images were processed and analyzed for fluorescence intensity of FLAG-HDAC4 using ImageJ (1.52k; National Institutes of Health). To measure FLAG-HDAC4 fluorescence intensity in the glial nuclei, a mask was created using the GFP channel to select only the areas comprising glial nuclei within the peripheral nerve. The mask was then applied to the stacks in which the FLAG channel had been isolated such that only FLAG signals within this nuclear mask were measured. To measure HDAC4 levels in the glial cytoplasm, the previously masked areas were subtracted from the total peripheral nerve to obtain the "non-nuclei" areas of glia. These regions were also analyzed for FLAG-HDAC4 fluorescence intensity, which was then divided by HDAC4 level of the glial nuclei within the peripheral nerve. This nuclear/cytoplasmic ratio of HDAC4 intensity was calculated for at least three different peripheral nerves of each larva and then averaged per animal, then per genotype. A minimum of 150 glial nuclei were examined for each genotype.

Transmission EM

To perform ultrastructural analysis of fly peripheral nerves, larvae were dissected in Ca^{2+}-free HL3.1 solution and fixed in 2% paraformaldehyde/2.5% glutaraldehyde (Polysciences) in 0.1 M PBS (pH 7.2) at 4°C overnight. On the following day, samples were washed with PBS and post-fixed in 0.5% osmium tetroxide (Polysciences)/0.08% potassium ferricyanide (Electron Microscopy Sciences) in 0.1 M PBS for 60 min, and then in 1% tannic acid (Electron Microscopy Sciences) in 0.1 M PBS for 60 min at room temperature. Subsequently, samples were washed extensively with distilled water before en bloc staining with 1% aqueous uranyl acetate (Ted Pella) for 60 min. After several rinses with water, samples were dehydrated in a graded series of ethanol and embedded in Eponate 12 resin (Ted Pella). Samples were then cut into 100-nm sections using a Leica Ultracut T ultramicrotome (Leica Microsystems), and stained with uranyl acetate and lead citrate. Electron micrographs were taken on a Hitachi H-7500 transmission electron microscope. Nonconsecutive sections from different nerves of four independent larvae were examined for each genotype.

Electrophysiology

To perform intracellular recordings, third instar larvae were dissected in freshly made Ca^{2+}-free HL3.1 buffer solution (70 mm NaCl, 5 mm KCl, 8 mm $MgCl_2$, 10 mm $NaHCO_3$, 5 mm trehalose, 5 mm HEPES, and 0 mm Ca^{2+}, pH 7.2; Feng et al., 2004). Larval preps were then rinsed with and recorded in HL3.1 solution containing 0.35 mM Ca^{2+}, unless otherwise noted. Spontaneous EJPs, evoked EJPs, and mEJPs were recorded from larval muscle 6 in segments A2, A3, and A4 using borosilicate sharp electrodes (15–20 MΩ). To determine amplitudes and frequencies of mEJP and spontaneous EJP, a minimum of 50 consecutive events were analyzed using MiniAnalysis Software (Synaptosoft) over a passive recording window, up to 75 consecutive events, or a total recording window of 120 s, whichever occurred first. To calculate spontaneous EJP frequency, first the exact length of recording was determined by subtracting the time of the first measured event from the time of the last measured event. Then, all events measured within the recording were filtered by amplitude: all events >4 mV were classified as "spontaneous EJPs," and the number of these events was divided by the exact length of recording to calculate the spontaneous EJP frequency value. Evoked EJPs were recorded by sucking the end of a severed segmental nerve into a stimulating electrode, followed by stimulation with a 1-ms pulse that had sufficient amperage to recruit both axons innervating muscle 6. To calculate EJP mean amplitude, 75 consecutive evoked events at 2 Hz were measured using pClamp9 software (Molecular Devices). For TTX experiments, TTX (1 μM; Sigma-Aldrich; T5651) was introduced to the recording solution only after spontaneous activity or evoked response to the initial pulse had been observed. In all experiments, intracellular recordings were used only if the resting membrane potential could be maintained at between −60 and −80 mV through the duration of the recording and the muscle input resistance was larger than 5 MΩ.

Behavioral analysis

To perform the bang-sensitive behavioral test, adult virgin female flies were collected within 24 h of eclosion (Ganetzky and Wu, 1982). After 2 h of resting on food, they were transferred to empty vials and mechanically stimulated for 15 s with a vortex mixer (Thermo Fisher Scientific) set at its maximum speed. The flies were assessed for seizure-like behaviors that lasted for at least 1 s, including shuddering, leg shaking, spinning flight, and contorted posture. Flies were tested in groups of 5–10, and at least 50 flies were assayed for each genotype and condition. The number of flies that exhibited seizure activity was counted at 10-s intervals, and the percentage of flies seizing was calculated for each time point on a 2-min time course.

Quantitative RT-PCR analysis

Larvae were dissected in 4°C PBS before their ventral nerve cords were isolated. 8–10 ventral nerve cord samples were incubated in TRIzol reagent (Thermo Fisher Scientific; 15596026) for 5 min and homogenized. The manufacturer's instructions were subsequently followed to extract RNA, and purified samples were Nanodropped for their RNA concentrations. Equal amounts of RNA from each genotype in a given experiment were treated with DNase (Sigma-Aldrich; DN25-1G) to eliminate genomic DNA and used to synthesize cDNA with the Quanta Biosciences qScript cDNA synthesis kit (VWR; 733–1177). PCR was performed to probe for the presence of sequences of interest in the cDNA samples. PCR products were run on a 2% agarose gel and imaged using G:Box Chemi-XX6 (Syngene). cDNA was diluted for quantitative RT-PCR analysis with Quanta Biosciences PerfeCTa SYBR Green FastMix with Rox. For data analysis, the

ΔΔCT method was used to calculate the mRNA fold change for each gene of interest between genotypes. Data were normalized to the mRNA levels of *rp49*. Quantification represents three independent biological replicates. The primer sequences used in this study were as follows: *Rp49* forward 5′-TACAGGCCCAAGATCGTGAAG-3′; *Rp49* reverse 5′-GACGCACTCTGTTGTCGATACC-3′; *SIK3* forward 5′-ACTCAGCCAGTTCCCTACTAT-3′; *SIK3* reverse 5′-AATGAGCTGGCTCCCATAAC-3′; *Fray* forward 5′-ACGTGGTGACCTATCACACCT-3′; *Fray* reverse 5′-CAGTTGGACGTTCGCATCTTG-3′; *Drip* forward 5′-TTGGCGTTGCCGACATAAC-3′; *Drip* reverse 5′-CGATTTGTGGTACACTTCCGC-3′; *Mlp84B* forward 5′-TGCGGCAAGAGTGTCTACG-3′; and *Mlp84B* reverse 5′-TCCAGGGATTTGTTGCACATT-3′.

HDAC inhibitor experiments

Trichostatin A (Selleck Chemicals; S1045) was resuspended from powder using DMSO and stored at −80°C as 10 mM aliquots. Before each experiment, the drug was further diluted and added to freshly made Formula 4–24 Instant Drosophila Medium Blue Food (Carolina; 173210) to reach a final concentration of 10 µM. For larval experiments, eggs were laid on Blue Food such that larvae were always exposed to the drug until being assessed on peripheral nerve morphology. Control experiments were performed by raising larvae of the same genotypes on Blue Food containing DMSO. For adult experiments, all genotypes were raised on control food until adulthood and collected within 24 h after eclosion. Adult flies were then immediately moved onto Blue Food with either DMSO or TSA for a 2-d treatment before being assessed in the bang-sensitive test.

Experimental design and statistical analysis

All *n* numbers represent biological replicates. For immunostaining experiments, to control for individual variability between larvae, a minimum of 10 larvae were assessed for each genotype and treatment condition. Each animal is considered an *n* of 1. For electrophysiological experiments, each NMJ is considered an *n* of 1, because each motor neuron is confined to its own muscle. In these studies, data were collected from multiple cells derived from a minimum of four different larvae. With the exception of behavioral tests, in which only adult virgin females were used, males and female larvae were used in comparable numbers. There are no statistical differences in nerve morphology or physiology between males and females.

Data are presented as mean ± SEM. Data were tested for normality using the D'Agostino–Pearson test and the Shapiro–Wilk test before being evaluated for statistical significance. Prism (7.02, GraphPad) was used to perform all statistical analyses, including one-way ANOVA test with Tukey's multiple comparisons, two-way ANOVA test with Tukey's multiple comparisons, and unpaired two-tailed Student's *t* test with unequal variance. Detailed information on *n* for each experiment, statistical test used, and P values can be found in the figure legends. Quantifications represent data from at least three independent experiments using larvae or adult flies derived from separately made crosses. In all studies, experimenters were blinded to genotype and treatment condition until data analysis was complete.

Conclusions

Disrupted K^+ buffering is a common underlying defect in epilepsy and ischemia that promotes neuronal hyperexcitability and edema. Glia play an essential role in K^+ and water homeostasis, raising hopes that glial mechanisms could be leveraged to treat disorders of hyperexcitability and edema. While many important glial ion and water transporters have been identified, global mechanisms regulating the glial capacity to buffer ions and water are not well understood. Here we uncover a signaling pathway that controls the glial capacity to maintain K^+ and water homeostasis via the regulated transcription of ion and water transport molecules. We identify SIK3 as the central regulator of this pathway, controlling the localization and thereby the function of HDAC4 as a negative regulator of a Mef2 transcriptional program that includes key effectors of K^+ and water homeostasis. This finding raises three key questions. First, in other contexts SIK3 integrates extracellular signals to control homeostatic transcriptional programs. What upstream signals work through SIK3 to regulate this glial program? Identifying such signals will help to answer the second question—what is the purpose of this glia regulatory mechanism? Since buffering K^+ and water is an essential glial function, one imagines it should be constitutively activated. We suggest that a bidirectional signaling system would provide glia with the ability to up-regulate buffering capacity in response to elevated neuronal activity, but then to down-regulate capacity during sustained hyperexcitability. This down-regulation would be a protective response ensuring that an excessive K^+ load doesn't result in pathological glial swelling. Finally, can the identification of this SIK3-HDAC4-Mef2 signaling pathway be leveraged to enhance K^+ buffering and pave the way for glial-centric therapeutic strategies to treat conditions associated with K^+ imbalance and hyperexcitability? Our demonstration that an HDAC inhibitor treats edema, hyperexcitability, and seizures suggests that such an approach has promise.

Online supplemental material

Fig. S1 contains representative images of larval peripheral nerves showing that SIK3 functions mainly in the wrapping glial layer to regulate extracellular ionic balance and is largely dispensable for the structural integrity of axons, and that the swellings in *SIK3* mutant peripheral nerve are extracellular. Fig. S2 shows that while control larvae are able to maintain a healthy nerve volume under high K^+ diets, larvae deprived of glial SIK3 are vulnerable to such K^+ stress. Fig. S3 shows that genetic deletion of SIK3 or pharmacological inhibition of HDAC does not significantly impact evoked synaptic transmission. Table S1 contains the list of genes tested in the in vivo glial-specific RNAi screen.

Acknowledgments

We thank Wandy Beatty at the Washington University Molecular Microbiology Imaging Facility for assistance with EM, and Amber Hackett of the Milbrandt laboratory for help with image analysis. We are also grateful to all members of the DiAntonio laboratory for helpful discussions and support.

This work was supported by funding from the National Institutes of Health (NS065053) to A. DiAntonio and the American Heart Association (18PRE34030101) to H. Li.

The authors declare no competing financial interests.

Author contributions: H. Li and A. DiAntonio conceived the project, designed the experiments, and wrote the manuscript. H. Li carried out the research and analyzed the data. A. Russo performed electrophysiology experiments and data analysis.

Submitted: 18 July 2019
Revised: 27 August 2019
Accepted: 19 September 2019

References

Auld, V.J., R.D. Fetter, K. Broadie, and C.S. Goodman. 1995. Gliotactin, a novel transmembrane protein on peripheral glia, is required to form the blood-nerve barrier in Drosophila. *Cell.* 81:757–767. https://doi.org/10.1016/0092-8674(95)90537-5

Bedner, P., A. Dupper, K. Hüttmann, J. Müller, M.K. Herde, P. Dublin, T. Deshpande, J. Schramm, U. Häussler, C.A. Haas, et al. 2015. Astrocyte uncoupling as a cause of human temporal lobe epilepsy. *Brain.* 138: 1208–1222. https://doi.org/10.1093/brain/awv067

Bellot-Saez, A., O. Kékesi, J.W. Morley, and Y. Buskila. 2017. Astrocytic modulation of neuronal excitability through K^+ spatial buffering. *Neurosci. Biobehav. Rev.* 77:87–97. https://doi.org/10.1016/j.neubiorev.2017.03.002

Blanchard, F.J., B. Collins, S.A. Cyran, D.H. Hancock, M.V. Taylor, and J. Blau. 2010. The transcription factor Mef2 is required for normal circadian behavior in Drosophila. *J. Neurosci.* 30:5855–5865. https://doi.org/10.1523/JNEUROSCI.2688-09.2010

Byun, N., and E. Delpire. 2007. Axonal and periaxonal swelling precede peripheral neurodegeneration in KCC3 knockout mice. *Neurobiol. Dis.* 28: 39–51. https://doi.org/10.1016/j.nbd.2007.06.014

Cabrero, P., S. Terhzaz, M.F. Romero, S.A. Davies, E.M. Blumenthal, and J.A.T. Dow. 2014. Chloride channels in stellate cells are essential for uniquely high secretion rates in neuropeptide-stimulated *Drosophila* diuresis. *Proc. Natl. Acad. Sci. USA.* 111:14301–14306. https://doi.org/10.1073/pnas.1412706111

Choi, S., D.-S. Lim, and J. Chung. 2015. Feeding and Fasting Signals Converge on the LKB1-SIK3 Pathway to Regulate Lipid Metabolism in Drosophila. *PLoS Genet.* 11:e1005263. https://doi.org/10.1371/journal.pgen.1005263

Devinsky, O., A. Vezzani, S. Najjar, N.C. De Lanerolle, and M.A. Rogawski. 2013. Glia and epilepsy: excitability and inflammation. *Trends Neurosci.* 36:174–184. https://doi.org/10.1016/j.tins.2012.11.008

Djukic, B., K.B. Casper, B.D. Philpot, L.-S. Chin, and K.D. McCarthy. 2007. Conditional knock-out of Kir4.1 leads to glial membrane depolarization, inhibition of potassium and glutamate uptake, and enhanced short-term synaptic potentiation. *J. Neurosci.* 27:11354–11365. https://doi.org/10.1523/JNEUROSCI.0723-07.2007

Feng, Y., A. Ueda, and C.-F. Wu. 2004. A modified minimal hemolymph-like solution, HL3.1, for physiological recordings at the neuromuscular junctions of normal and mutant *Drosophila* larvae. *J. Neurogenet.* 18: 377–402. https://doi.org/10.1080/01677060490894522

Fitzsimons, H.L., S. Schwartz, F.M. Given, and M.J. Scott. 2013. The histone deacetylase HDAC4 regulates long-term memory in Drosophila. *PLoS One.* 8:e83903. https://doi.org/10.1371/journal.pone.0083903

Fujii, S., P. Emery, and H. Amrein. 2017. SIK3-HDAC4 signaling regulates *Drosophila* circadian male sex drive rhythm via modulating the DN1 clock neurons. *Proc. Natl. Acad. Sci. USA.* 114:E6669–E6677. https://doi.org/10.1073/pnas.1620483114

Ganetzky, B., and C.F. Wu. 1982. Indirect Suppression Involving Behavioral Mutants with Altered Nerve Excitability in DROSOPHILA MELANOGASTER. *Genetics.* 100:597–614.

Ganetzky, B., and C.F. Wu. 1983. Neurogenetic analysis of potassium currents in Drosophila: synergistic effects on neuromuscular transmission in double mutants. *J. Neurogenet.* 1:17–28. https://doi.org/10.3109/01677068309107069

Han, C., L.Y. Jan, and Y.-N. Jan. 2011. Enhancer-driven membrane markers for analysis of nonautonomous mechanisms reveal neuron-glia interactions in Drosophila. *Proc. Natl. Acad. Sci. USA.* 108:9673–9678. https://doi.org/10.1073/pnas.1106386108

Heuser, K., K. Szokol, and E. Taubøll. 2014. The role of glial cells in epilepsy. *Tidsskr. Nor. Laegeforen.* 134:37–41. https://doi.org/10.4045/tidsskr.12.1344

Jayakumar, A.R., K.S. Panickar, K.M. Curtis, X.Y. Tong, M. Moriyama, and M.D. Norenberg. 2011. Na-K-Cl cotransporter-1 in the mechanism of cell swelling in cultured astrocytes after fluid percussion injury. *J. Neurochem.* 117:437–448. https://doi.org/10.1111/j.1471-4159.2011.07211.x

Kofuji, P., and E.A. Newman. 2004. Potassium buffering in the central nervous system. *Neuroscience.* 129:1045–1056. https://doi.org/10.1016/j.neuroscience.2004.06.008

Kuebler, D., H. Zhang, X. Ren, and M.A. Tanouye. 2001. Genetic suppression of seizure susceptibility in Drosophila. *J. Neurophysiol.* 86:1211–1225. https://doi.org/10.1152/jn.2001.86.3.1211

Larsen, B.R., M. Assentoft, M.L. Cotrina, S.Z. Hua, M. Nedergaard, K. Kaila, J. Voipio, and N. MacAulay. 2014. Contributions of the Na^+/K^+-ATPase, NKCC1, and Kir4.1 to hippocampal K^+ clearance and volume responses. *Glia.* 62:608–622. https://doi.org/10.1002/glia.22629

Lee, D.J., M.S. Hsu, M.M. Seldin, J.L. Arellano, and D.K. Binder. 2012. Decreased expression of the glial water channel aquaporin-4 in the intrahippocampal kainic acid model of epileptogenesis. *Exp. Neurol.* 235: 246–255. https://doi.org/10.1016/j.expneurol.2012.02.002

Leiserson, W.M., and H. Keshishian. 2011. Maintenance and regulation of extracellular volume and the ion environment in Drosophila larval nerves. *Glia.* 59:1312–1321. https://doi.org/10.1002/glia.21132

Leiserson, W.M., E.W. Harkins, and H. Keshishian. 2000. Fray, a Drosophila serine/threonine kinase homologous to mammalian PASK, is required for axonal ensheathment. *Neuron.* 28:793–806. https://doi.org/10.1016/S0896-6273(00)00154-9

Leiserson, W.M., B. Forbush, and H. Keshishian. 2011. Drosophila glia use a conserved cotransporter mechanism to regulate extracellular volume. *Glia.* 59:320–332. https://doi.org/10.1002/glia.21103

MacVicar, B.A., D. Feighan, A. Brown, and B. Ransom. 2002. Intrinsic optical signals in the rat optic nerve: role for K(+) uptake via NKCC1 and swelling of astrocytes. *Glia.* 37:114–123. https://doi.org/10.1002/glia.10023

Min, R., and M.S. van der Knaap. 2018. Genetic defects disrupting glial ion and water homeostasis in the brain. *Brain Pathol.* 28:372–387. https://doi.org/10.1111/bpa.12602

Noebels, J.L., M. Avoli, M.A. Rogawski, R.W. Olsen, and A.V. Delgado-Escueta, editors. 2012. *Jasper's Basic Mechanisms of the Epilepsies.* Fourth edition. National Center for Biotechnology Information, Bethesda, MD.

Paciorkowski, A.R., R.N. Traylor, J.A. Rosenfeld, J.M. Hoover, C.J. Harris, S. Winter, Y. Lacassie, M. Bialer, A.N. Lamb, R.A. Schultz, et al. 2013. MEF2C Haploinsufficiency features consistent hyperkinesis, variable epilepsy, and has a role in dorsal and ventral neuronal developmental pathways. *Neurogenetics.* 14:99–111. https://doi.org/10.1007/s10048-013-0356-y

Papadopoulos, M.C., G.T. Manley, S. Krishna, and A.S. Verkman. 2004. Aquaporin-4 facilitates reabsorption of excess fluid in vasogenic brain edema. *FASEB J.* 18:1291–1293. https://doi.org/10.1096/fj.04-1723fje

Parker, L., I.C. Howlett, Z.M. Rusan, and M.A. Tanouye. 2011. Seizure and Epilepsy: Studies of Seizure Disorders in Drosophila. *In International Review of Neurobiology*. Vol. 99. Elsevier. pp. 1–21.

Pavlidis, P., and M.A. Tanouye. 1995. Seizures and failures in the giant fiber pathway of Drosophila bang-sensitive paralytic mutants. *J. Neurosci.* 15: 5810–5819. https://doi.org/10.1523/JNEUROSCI.15-08-05810.1995

Phiel, C.J., F. Zhang, E.Y. Huang, M.G. Guenther, M.A. Lazar, and P.S. Klein. 2001. Histone deacetylase is a direct target of valproic acid, a potent anticonvulsant, mood stabilizer, and teratogen. *J. Biol. Chem.* 276: 36734–36741. https://doi.org/10.1074/jbc.M101287200

Reddy, S.D., B.L. Clossen, and D.S. Reddy. 2018. Epigenetic Histone Deacetylation Inhibition Prevents the Development and Persistence of Temporal Lobe Epilepsy. *J. Pharmacol. Exp. Ther.* 364:97–109. https://doi.org/10.1124/jpet.117.244939

Rusan, Z.M., O.A. Kingsford, and M.A. Tanouye. 2014. Modeling glial contributions to seizures and epileptogenesis: cation-chloride cotransporters in Drosophila melanogaster. *PLoS One.* 9:e101117. https://doi.org/10.1371/journal.pone.0101117

Sandmann, T., L.J. Jensen, J.S. Jakobsen, M.M. Karzynski, M.P. Eichenlaub, P. Bork, and E.E.M. Furlong. 2006. A temporal map of transcription factor activity: mef2 directly regulates target genes at all stages of muscle development. *Dev. Cell.* 10:797–807. https://doi.org/10.1016/j.devcel.2006.04.009

Sando, R. III, N. Gounko, S. Pieraut, L. Liao, J. Yates III, and A. Maximov. 2012. HDAC4 governs a transcriptional program essential for synaptic plasticity and memory. *Cell.* 151:821–834. https://doi.org/10.1016/j.cell.2012.09.037

Sasagawa, S., H. Takemori, T. Uebi, D. Ikegami, K. Hiramatsu, S. Ikegawa, H. Yoshikawa, and N. Tsumaki. 2012. SIK3 is essential for chondrocyte hypertrophy during skeletal development in mice. *Development.* 139: 1153–1163. https://doi.org/10.1242/dev.072652

Schwartz, S., M. Truglio, M.J. Scott, and H.L. Fitzsimons. 2016. Long-Term Memory in *Drosophila* Is Influenced by Histone Deacetylase HDAC4 Interacting with SUMO-Conjugating Enzyme Ubc9. *Genetics.* 203: 1249–1264. https://doi.org/10.1534/genetics.115.183194

Sepp, K.J., J. Schulte, and V.J. Auld. 2001. Peripheral glia direct axon guidance across the CNS/PNS transition zone. *Dev. Biol.* 238:47–63. https://doi.org/10.1006/dbio.2001.0411

Sivachenko, A., Y. Li, K.C. Abruzzi, and M. Rosbash. 2013. The transcription factor Mef2 links the Drosophila core clock to Fas2, neuronal morphology, and circadian behavior. *Neuron.* 79:281–292. https://doi.org/10.1016/j.neuron.2013.05.015

Stenesen, D., A.T. Moehlman, J.N. Schellinger, A.R. Rodan, and H. Krämer. 2019. The glial sodium-potassium-2-chloride cotransporter is required for synaptic transmission in the Drosophila visual system. *Sci. Rep.* 9: 2475. https://doi.org/10.1038/s41598-019-38850-x

Stork, T., D. Engelen, A. Krudewig, M. Silies, R.J. Bainton, and C. Klämbt. 2008. Organization and function of the blood-brain barrier in Drosophila. *J. Neurosci.* 28:587–597. https://doi.org/10.1523/JNEUROSCI.4367-07.2008

Strohschein, S., K. Hüttmann, S. Gabriel, D.K. Binder, U. Heinemann, and C. Steinhäuser. 2011. Impact of aquaporin-4 channels on K+ buffering and gap junction coupling in the hippocampus. *Glia.* 59:973–980. https://doi.org/10.1002/glia.21169

Stronach, B.E., P.J. Renfranz, B. Lilly, and M.C. Beckerle. 1999. Muscle LIM proteins are associated with muscle sarcomeres and require dMEF2 for their expression during Drosophila myogenesis. *Mol. Biol. Cell.* 10: 2329–2342. https://doi.org/10.1091/mbc.10.7.2329

Sun, B., P. Xu, and P.M. Salvaterra. 1999. Dynamic visualization of nervous system in live Drosophila. *Proc. Natl. Acad. Sci. USA.* 96:10438–10443. https://doi.org/10.1073/pnas.96.18.10438

Uebi, T., Y. Itoh, O. Hatano, A. Kumagai, M. Sanosaka, T. Sasaki, S. Sasagawa, J. Doi, K. Tatsumi, K. Mitamura, et al. 2012. Involvement of SIK3 in glucose and lipid homeostasis in mice. *PLoS One.* 7:e37803. https://doi.org/10.1371/journal.pone.0037803

Wang, B., N. Moya, S. Niessen, H. Hoover, M.M. Mihaylova, R.J. Shaw, J.R. Yates III, W.H. Fischer, J.B. Thomas, and M. Montminy. 2011. A hormone-dependent module regulating energy balance. *Cell.* 145: 596–606. https://doi.org/10.1016/j.cell.2011.04.013

Wang, Z., G. Qin, and T.C. Zhao. 2014. HDAC4: mechanism of regulation and biological functions. *Epigenomics.* 6:139–150. https://doi.org/10.2217/epi.13.73

Weiss, S., J.E. Melom, K.G. Ormerod, Y.V. Zhang, and J.T. Littleton. 2019. Glial Ca^{2+}signaling links endocytosis to K^+ buffering around neuronal somas to regulate excitability. *eLife.* 8:e44186. https://doi.org/10.7554/eLife.44186

Wu, Q., Y.-J. Zhang, J.-Y. Gao, X.-M. Li, H. Kong, Y.-P. Zhang, M. Xiao, C.B. Shields, and G. Hu. 2014. Aquaporin-4 mitigates retrograde degeneration of rubrospinal neurons by facilitating edema clearance and glial scar formation after spinal cord injury in mice. *Mol. Neurobiol.* 49: 1327–1337. https://doi.org/10.1007/s12035-013-8607-3

Xie, X., and V.J. Auld. 2011. Integrins are necessary for the development and maintenance of the glial layers in the Drosophila peripheral nerve. *Development.* 138:3813–3822. https://doi.org/10.1242/dev.064816

Yao, K.M., and K. White. 1994. Neural specificity of elav expression: defining a Drosophila promoter for directing expression to the nervous system. *J. Neurochem.* 63:41–51. https://doi.org/10.1046/j.1471-4159.1994.63010041.x